

OUTER-DISK POPULATIONS IN NGC 7793: EVIDENCE FOR STELLAR RADIAL MIGRATION

DAVID J. RADBURN-SMITH¹, ROK ROŠKAR², VICTOR P. DEBATTISTA³, JULIANNE J. DALCANTON¹, DAVID STREICH⁴,
ROELOF S. DE JONG⁴, MARIJA VLAJIĆ⁴, BENNE W. HOLWERDA⁵, CHRIS W. PURCELL⁶,
ANDREW E. DOLPHIN⁷, AND DANIEL B. ZUCKER^{8,9}

Accepted for publication in ApJ

ABSTRACT

We analyzed the radial surface brightness profile of the spiral galaxy NGC 7793 using *HST*/ACS images from the GHOSTS survey and a new *HST*/WFC3 image across the disk break. We used the photometry of resolved stars to select distinct populations covering a wide range of stellar ages. We found breaks in the radial profiles of all stellar populations at $280''$ (~ 5.1 kpc). Beyond this disk break, the profiles become steeper for younger populations. This same trend is seen in numerical simulations where the outer disk is formed almost entirely by radial migration. We also found that the older stars of NGC 7793 extend significantly farther than the underlying H I disk. They are thus unlikely to have formed entirely at their current radii, unless the gas disk was substantially larger in the past. These observations thus provide evidence for substantial stellar radial migration in late-type disks.

Keywords: galaxies: evolution — galaxies: spiral — galaxies: stellar content — galaxies: structure — techniques: photometric

1. INTRODUCTION

Studies of the chemical composition of galaxy disks typically assume that the orbital radii of stars are essentially static. Only a small diffusion in radial distance, increasing with age, is expected due to dynamical heating (e.g., Wielen 1977; Dehnen & Binney 1998). In this scenario, the metallicity of stars of similar age and galactic distance should be comparable, as they are born from the remnants of previous stellar generations that orbited at the same radius. However, observations of local F and G dwarfs have found little evidence for such coexistent evolution, instead revealing a large scatter in the age–metallicity distribution (Edvardsson et al. 1993). Theoretical work has suggested that this scatter may be due to resonant interactions between stars and spiral arms, which enable stars to migrate across many kpc (Sellwood & Binney 2002). Indeed, using a high-resolution hydrodynamical simulation, Roškar et al. (2008a) found that such migration naturally led to the high degree of variation observed in the age–metallicity relation of local Milky Way (MW) stars. These events, in which the guiding center of the star shifts, differ from general diffusion where the epicyclic motion increases by only a few kpc due to an increase in velocity dispersion.

Testing such models of stellar migration may be possible using studies of stellar populations beyond the classical disk break of late-type galaxies. The cause of this break is still de-

bated (see the review by Trujillo & Pohlen 2005), however the change in surface brightness is often associated with a threshold in the star formation rate (SFR; e.g., van der Kruit & Searle 1981; Kennicutt 1989; Schaye 2004; Elmegreen & Hunter 2006). Using a study of 85 late-type galaxies, Pohlen & Trujillo (2006) found that the surface brightness profile of approximately 60% of disk galaxies steepens beyond the disk break. Hence, the outskirts of disk galaxies are often associated with a dearth of star formation. Using *N*-body simulations of disk galaxy formation, Roškar et al. (2008b) found that if star formation is sufficiently suppressed beyond the break, then that region may form almost entirely from stars migrated from the inner disk. This would leave a clear signal on radial surface brightness profiles, with older stars (i.e., those that have been subject to scattering for longer) exhibiting shallower profiles.

Observations from the GHOSTS¹⁰ survey (Radburn-Smith et al. 2011, hereafter R-S11), which have targeted the outskirts of several nearby disk galaxies using the *Hubble Space Telescope* Advanced Camera for Surveys (*HST*/ACS), thus offer a significant test of radial migration. GHOSTS observations of NGC 4244 revealed the location of the disk break to be independent of stellar age, thus constraining several mechanisms for the formation of this feature (de Jong et al. 2007). However, lack of data beyond the break prevented further analysis. In this paper, we focus on the spiral galaxy NGC 7793. This flocculent galaxy is (1) relatively nearby (3.7 ± 0.1 Mpc, R-S11), (2) situated at high Galactic latitude (-77.2°) and hence relatively uncontaminated by foreground stars, and (3) an isolated loosely bound member of the Sculptor Group. NGC 7793 was recently studied by Vlahić et al. (2011), who found no sign of a break in the red giant branch (RGB) population, but did find evidence for an upturn in the radial metallicity distribution beyond the disk break. In this paper, we expand on this work by using data from the GHOSTS survey together with a new *HST* Wide Field Camera 3 (WFC3) image of the inner disk to measure fainter stars and to recover stellar densities in this crowded region. We

¹ Department of Astronomy, University of Washington, Seattle, WA 98195, USA

² Institut für Theoretische Physik, Universität Zürich, Switzerland

³ RCUK Fellow. Jeremiah Horrocks Institute, University of Central Lancashire, Preston, PR1 2HE, UK

⁴ Leibniz-Institut für Astrophysik Potsdam, D-14482 Potsdam, Germany

⁵ European Space Agency, ESTEC, 2200 AG Noordwijk, The Netherlands

⁶ Department of Physics and Astronomy, University of Pittsburgh, Pittsburgh, PA 15260, USA

⁷ Raytheon, 1151 E. Hermans Road, Tucson, AZ 85756, USA

⁸ Department of Physics and Astronomy, Macquarie University, NSW 2109, Australia

⁹ Australian Astronomical Observatory, NSW 1710, Australia

¹⁰ Galaxy Halos, Outer disks, Substructure, Thick disks, and Star clusters.

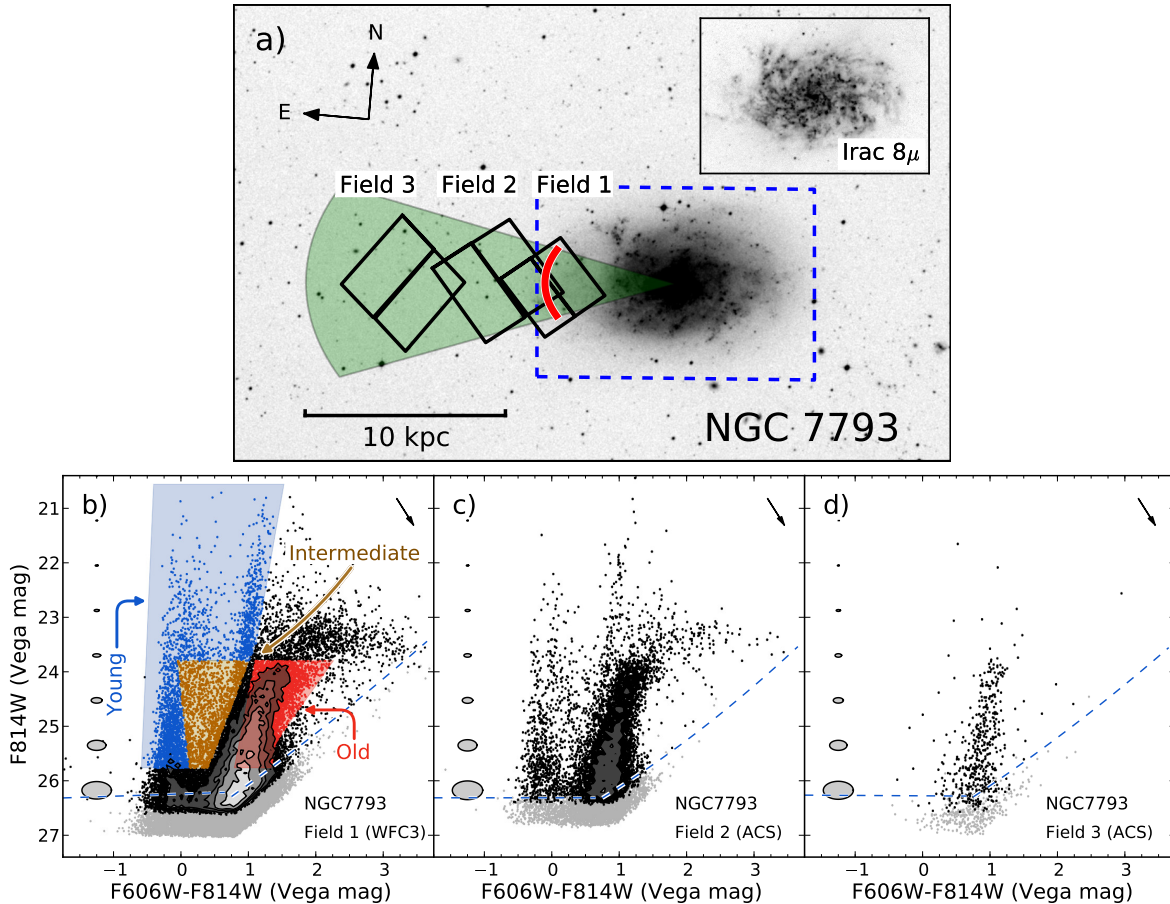


Figure 1. Location of the observations and resulting color magnitude diagrams (CMDs). Radial surface brightness profiles are taken from the shaded wedge (with a de-projected opening angle of 25°) in panel (a). The thick red line marks the disk break. The blue dashed region denotes the area covered by the *Spitzer*/IRAC 8μ observation in the top right inset, which highlights the spiral structure that may be responsible for stellar migration. Panels (b)–(d) plot the individual CMDs, with the regions used to extract the different stellar populations, as described in the text, highlighted in panel (b). Gray and black points indicate different cuts on the signal-to-noise ratio of 3.5 and 5.0, respectively, with contours drawn at densities of 50, 100, 150, and 250 stars per 0.01 mag^2 . The black arrows indicate the direction of reddening due to foreground extinction, which has been removed from the data. The shaded ellipses indicate photometric errors as reported by DOLPHOT, and the blue dashed lines mark the 50% completeness limits calculated from artificial star tests.

compare these observations with predictions from the radial migration simulations of Roškar et al. (2008b) and discuss alternate explanations.

2. *HST* ACS/WFC3 PHOTOMETRY

Figure 1 plots the location of the two GHOSTS fields discussed in this paper (Fields 2 and 3). Each field was observed with dithered 740 s exposures in both the F606W and F814W filters. R-S11 described the data reduction and photometry of the resolved stars in these fields using the DOLPHOT code (Dolphin 2000). A further field (Field 1) was observed with the WFC3 camera to characterize the disk truncation (*HST* GO program 12196). This observation was made using the same filters as the ACS fields, with dithered exposures of 980 s in F606W and 1488 s in F814W. We use the same DOLPHOT parameters and the same crowded-field stellar selection criteria for the WFC3 field as used by R-S11 for the ACS photometry. Despite minor differences between the cameras, namely, pixel scale and quantum efficiency in the F814W filter, we found little discrepancy in the resulting photometry between the cameras in overlapping regions.

The resulting color magnitude diagrams (CMDs) for each of the fields are presented in Figure 1. By analyzing synthetic CMDs generated with a constant SFR of $0.01 M_\odot$

yr^{-1} , an appropriate metallicity of $[\text{Fe}/\text{H}] = -1$, and photometric errors matching the observations, we identified three regions of the CMD corresponding to three discrete age ranges. The area marked as “Young” consists of bright main sequence and helium-burning (HeB) stars, which are collectively 10–100 Myr old; the “Intermediate” region is composed of 100 Myr–1 Gyr old HeB stars; and the “Old” region consists of 1–10 Gyr old RGB stars. We subsequently use these regions, which suffer little cross contamination, to select stellar populations by age.

R-S11 generated artificial stars for the ACS fields, which were subsequently used to assess errors and correct for completeness due to stellar crowding. We generated an additional 1.8 million artificial stars for the WFC3 image. Figure 1 plots the 50% recovery limit of these artificial stars, which we set as our limiting magnitude.

We found good agreement between detection rates and photometry in the overlapping region of Fields 1 and 2. The WFC3 observation from Field 1 yielded 3474 detections brighter than $F814W = 25.75\text{ mag}$ after culling, while ACS (Field 2) found 3631, despite the shorter exposure time. Approximately 82% of the ACS detections were coincident between fields. After correcting for completeness with the artificial star tests, this increased to 95%. The remainder can

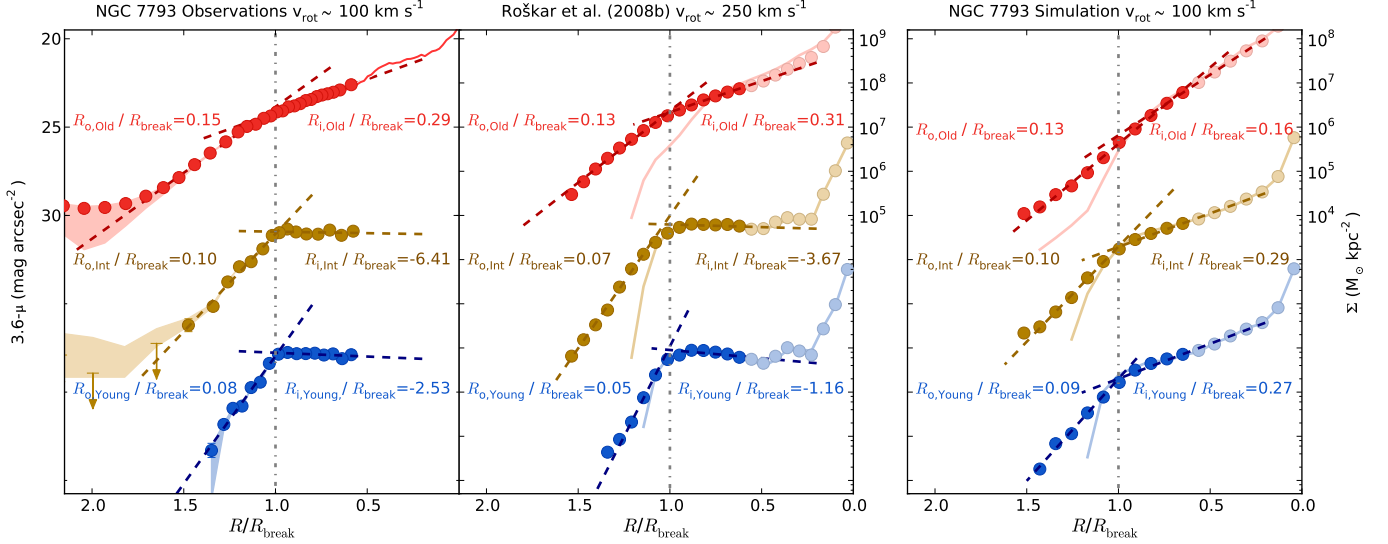


Figure 2. Radial surface brightness profiles of “Old” (red), “Intermediate” (yellow), and “Young” (blue) stellar populations. The left panel plots number counts in NGC 7793 taken from the shaded region of Figure 1, panel (a). The middle and right panels, respectively, plot surface densities extracted from similar regions of the Roškar et al. (2008b) simulation of a Milky Way (MW) sized galaxy and the new simulation of NGC 7793 described in the text. The NGC 7793 observations have been linearly offset such that the “Old” population matches a *Spitzer* 3.6 μm surface brightness profile, indicated by a solid red line. For clarity, the “Intermediate” and “Young” population are arbitrarily offset by 5 and 12.5 mag, respectively, in the observations, and by 2 and 4 dex in the simulations. All profiles are scaled to the approximate location of the “Young” break (280'' in NGC 7793, 10.2 kpc in the MW simulation, and 7.7 kpc in the NGC 7793 simulation). Arrows indicate where the Poisson uncertainty may move the data point below the background level. Dashed lines indicate exponential fits to the inner and outer profiles, with the corresponding normalized exponential-disk scale lengths given by R_i and R_o , respectively. The shaded regions in the left panel indicate the range of possible profiles due to different treatments of background contamination as described in the text. Faint solid lines in the simulation panels plot the radial surface brightness profiles using the formation radius of the stars, i.e., removing the effects of stellar migration.

be attributed to incompleteness at the magnitude limit of the survey. The median photometric differences between coincident detections are -0.05 and 0.03 mag in F606W and F814W, respectively. The mean error of these detections, when combined in quadrature, is ± 0.10 in both filters. Hence, although the offsets are systematic, they are significantly less than the DOLPHOT uncertainties. We thus found our photometry from the two different cameras to be consistent and complete to $F814W = 25.75$ mag.

3. RADIAL SURFACE BRIGHTNESS PROFILES

In the left panel of Figure 2, we plot the radial star counts of NGC 7793 within the shaded region of panel (a) of Figure 1 for our key stellar populations. These profiles are all normalized to the radial break observed in the youngest population. In addition to masking foreground stars and background galaxies, a region of significant star formation, located at $23^{\text{h}}58^{\text{m}}13^{\text{s}}.1$, $-32^{\circ}36'37''.3$ was masked out of Fields 1 and 2 to provide a better estimate of the mean surface brightness. We assigned an equivalent surface brightness to the star count profiles by multiplying the logarithm of the older RGB counts by 2.5 and linearly offsetting the result to match a *Spitzer* Infrared Array Camera (IRAC) 3.6 μm surface brightness profile extracted from the same region. Consequently, we find the star count profiles reach a limiting magnitude equivalent to ~ 32 AB mag arcsec $^{-2}$ at 3.6 μm .

Each of the stellar population bins denoted in panel (b) of Figure 1 are substantially brighter than the completeness limits. They are thus less susceptible to spurious detections from cosmic rays and CCD noise that become significant at a lower signal-to-noise ratio. Instead, contamination is expected from unresolved background galaxies, which far outnumber any foreground MW stars. To account for this, we followed the same analysis used by R-S11 and ran the photometry code on ACS images of high- z sources with exposure lengths longer

than our observations. As these fields are free of any resolvable stars outside of the MW, any detections will thus be contaminants, primarily from background galaxies. For each of the denoted stellar populations in panel (b) of Figure 1, we measured contamination from the number density of remaining detections in these “empty” archival fields after imposing the selection criteria used by R-S11. For the “Old”, “Intermediate”, and “Young” bins we recovered 4.4×10^{-4} , 4.0×10^{-4} , and 3.3×10^{-4} detections per arcsec 2 , respectively. Each of these contaminant measurements are lower than any of the detection rates in the corresponding NGC 7793 populations. Averaging the outermost radial bins of each population in NGC 7793, we, respectively, measured 4.0×10^{-3} , 4.5×10^{-4} , and 1.6×10^{-3} detections per arcsec 2 . As discussed in Ellis & Bland-Hawthorn (2007), these can be treated as upper limits on the true level of contaminants in each bin. Moreover, using the GALAXYCOUNT software described in Ellis & Bland-Hawthorn (2007), we can infer uncertainties on these values due to cosmic variance and Poisson noise. These equate to upper limits on the total number of background galaxies in an ACS/WFC field of 163 ± 14 , 18 ± 4 , and 65 ± 8 for the respective age bins. These uncertainties are incorporated into the final error we assign to the profiles. The lower bound on the profiles due to removing this higher level of contamination, as well as an upper bound resulting from not subtracting any contaminants, are indicated by the shaded regions in the left panel of Figure 2.

We are able to probe the outskirts of NGC 7793 much deeper than previous integrated light studies, whose profiles do not cover these radii or reach this surface brightness limit (e.g., Muñoz-Mateos et al. 2009; Vlajić et al. 2011). We consequently found that the disk break, R_{break} , occurs at approximately the same location regardless of the age of the underlying stars, in agreement with observations of the edge-on disk

Table 1
Exponential Outer-disk Fits

| Data Set | $R_{\text{old}}/R_{\text{break}}$ | $R_{\text{int}}/R_{\text{break}}$ | $R_{\text{young}}/R_{\text{break}}$ |
|-------------------------------|-----------------------------------|-----------------------------------|-------------------------------------|
| NGC 7793 Observations | | | |
| Raw | 0.147 ± 0.007 | 0.107 ± 0.016 | 0.078 ± 0.014 |
| Corrected | 0.145 ± 0.007 | 0.098 ± 0.016 | 0.075 ± 0.014 |
| Overcorrected | 0.134 ± 0.016 | 0.080 ± 0.017 | 0.063 ± 0.022 |
| Simulations | | | |
| Roškar et al. (2008b) | 0.134 ± 0.008 | 0.072 ± 0.007 | 0.053 ± 0.006 |
| NGC 7793 Model | 0.125 ± 0.012 | 0.101 ± 0.007 | 0.094 ± 0.007 |
| Simulations without Migration | | | |
| Roškar et al. (2008b) | 0.025 ± 0.018 | 0.018 ± 0.011 | 0.024 ± 0.014 |
| NGC 7793 Model | 0.054 ± 0.019 | 0.032 ± 0.011 | 0.025 ± 0.013 |

Note. — The “Raw” NGC 7793 observations refers to profiles uncorrected for contamination from background galaxies. For the “Overcorrected” profiles, an upper limit on the number of the contaminants is inferred from the average density of detections in the outermost radial bins of each stellar population in the raw data. The exponential-disk fits to the “Simulations without Migration” use the formation radii of stars born in the outer-disk region.

galaxy NGC 4244 (de Jong et al. 2007). This break occurs at $280''$ (5.1 kpc), internal to the regions covered by Vlajić et al. (2011) and external to the integrated light profiles of Muñoz-Mateos et al. (2009). de Jong et al. (2007) argued that a constant break location calls for a dynamical interpretation, given that a break radius due solely to a star formation threshold is unlikely to remain at the same radius over the lifetime of the galaxy, due to disk growth. We note that the break is weakest in the oldest population, which also shows a possible second break to a shallower profile around $\sim 1.8 \times R_{\text{break}}$. This may correspond to a transition in the number counts from a disk-dominated population to one composed primarily of stellar halo stars (see Section 5.1).

Although the disk break appears at a constant radius for all stellar ages, the profiles in Figure 2 suggest that the slope of the profile does depend on age, both within and beyond the break. We characterize this slope by fitting the inner and outer profiles to an exponential surface brightness function of the form $\mu(r) = \mu_0 e^{-R/R_d}$, where μ_0 is the central surface brightness and R_d is the exponential-disk scale length. The resulting fits, shown in Figure 2 and Table 1, reveal a smooth increase in the steepness of the outer profile with decreasing age, together with a corresponding flattening of the inner profile.

To assess the uncertainty in the profiles we use Monte Carlo realizations of the data. As summarized in Table 1, the outer-disk parameters of the “Old” population are robust ($\sim 5\%$ uncertainty), but low number counts in the “Intermediate” and “Young” outer-disk profiles leads to uncertainties of $\sim 16\%$ and $\sim 19\%$, respectively. Accounting for different levels of contamination has little effect on the fits.

4. COMPARISON WITH SIMULATIONS

In isolated simulations of a MW-type galaxy, Roškar et al. (2008b) found significant migration of stars over several kpc, such that $\sim 90\%$ of the outer disk was predominantly formed from migrated stars. Older populations exhibited larger scale lengths than younger populations, because the former were subject to migration for longer. We can compare our measured profiles to those of Roškar et al. (2008b), which are plotted in the middle panel of Figure 2 for the same age ranges used in our CMD analysis. These profiles were extracted from the simulation at the same inclination as NGC 7793 ($\sim 53^\circ$),

and for comparison with the observations are similarly scaled to the break radius of the youngest stellar population. The behavior of the profiles in the simulation is qualitatively similar to what is observed in the data. However, the simulation is not necessarily the best analog for NGC 7793. The mass of the simulation contained within 10 kpc is approximately $1.2 \times 10^{11} M_\odot$, larger than the mass of NGC 7793, which Carignan & Puche (1990) measure within 7.35 kpc as $1.5 \times 10^{10} M_\odot$. Similarly, the radius of the disk break is also larger in the simulation (10.2 kpc cf. 5.1 kpc in NGC 7793).

4.1. Modeling NGC 7793

A potentially better analog to NGC 7793 is the equivalent simulation generated to model NGC 300 in Gogarten et al. (2010). This galaxy is another member of the Sculptor Group with mass similar to NGC 7793, although the star formation history (SFH) of the system and the lack of a disk break indicate a quiescent formation. Gogarten et al. (2010) found little evidence of migration in *HST* observations of NGC 300, and less migration in the NGC 300 simulation than the Roškar et al. (2008b) model. This led the authors to suggest that both mass and environment may be factors in radial migration. As the formation of transient spiral structure is linked to gas accretion and star formation (Sellwood & Carlberg 1984), such a dependence on environment is to be expected. This was further demonstrated by Gogarten et al. (2010), who note that the comparably massive M 33, which is interacting with M 31, does show signs of radial diffusion (Williams et al. 2009).

We extend this analysis by observing that the *K*-band absolute surface brightness of NGC 7793 is on average ~ 1.0 mag arcsec $^{-2}$ brighter than NGC 300 (see panel (a) of Figure 3). The surface density of the NGC 300 disk may thus be too low to support the transient spiral structures required to drive substantial migration. To better match the properties of NGC 7793 we resimulated the NGC 300 model with a smaller spin parameter to yield a disk with a smaller scale length (Figure 3, panel (b)), larger rotational velocity (Figure 3, panel (d)), and higher surface density within the central 4 kpc. These changes resulted in a more concentrated system, with $1.7 \times 10^{10} M_\odot$ contained within the disk break (located at 7.7 kpc). The stellar disk in this model was also subject to significant radial migration, leading to a similar increase in disk scale length with stellar age as in the Roškar et al. (2008b) model (see right panel of Figure 2 and Table 1). The effect is, however, weaker. We partly attribute this difference to a relative increase in the level of in situ formation beyond the disk break in the NGC 7793 model. This is manifest in Figure 2 and Table 1 by exponential-disk fits to the formation radii of stars located beyond the break. Specifically, the normalized scale lengths are greater in the NGC 7793 model than in the MW simulation. The NGC 300 model generated by Gogarten et al. (2010) shows a further increase in this in situ population, which resulted in an even softer disk break.

Figure 4 compares the cumulative SFH of the main disk of NGC 7793 to the Roškar et al. (2008b) MW simulation and the new NGC 7793 simulation, both of which show signs of radial migration. To extract the SFH from the *HST*/ACS photometry, we used the software package MATCH (Dolphin 2002). This program uses a maximum likelihood analysis to fit the observed CMD with stars generated from the stellar evolution models of Girardi et al. (2002, with updated AGB models from Marigo et al. 2008 and Girardi et al. 2010, and assuming a Salpeter 1955 IMF and a binary fraction of

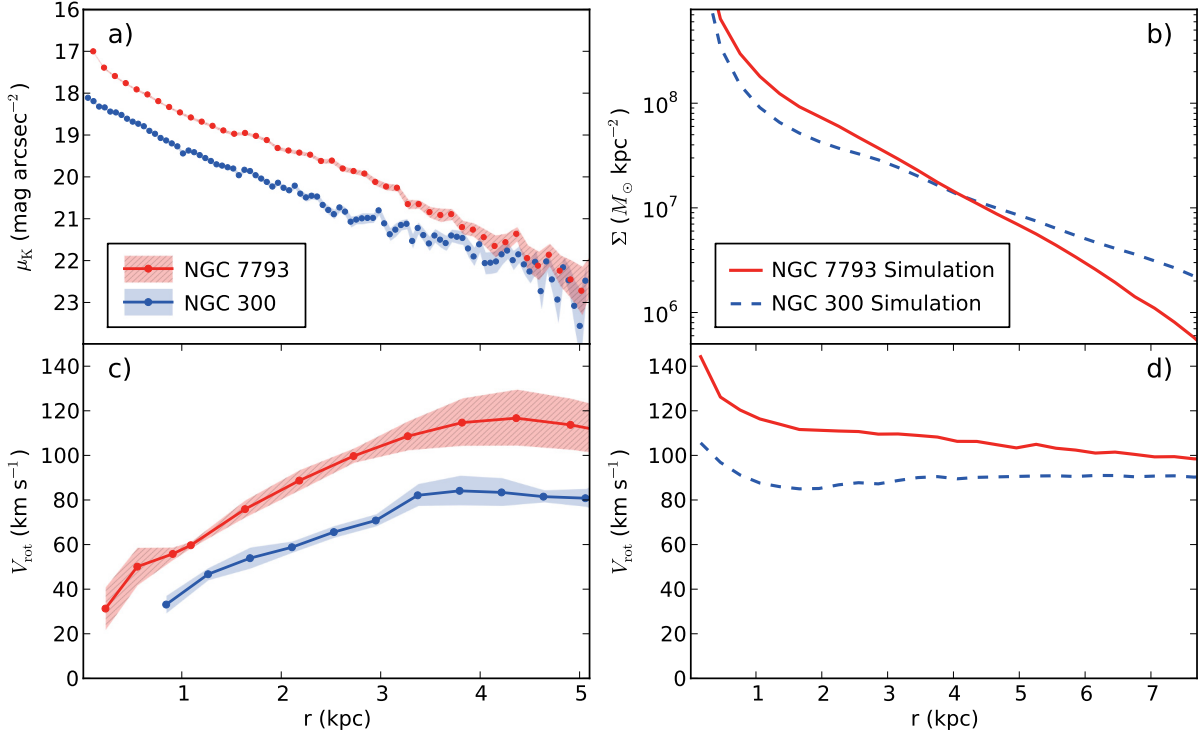


Figure 3. Radial surface brightness profiles (top panels) and H I rotational velocity profiles (bottom panels) from observations of NGC 7793 and NGC 300 (left panels) and from simulations of NGC 7793 and NGC 300 (right panels). The NGC 7793 simulation is described in the text while the NGC 300 simulation is taken from Gogarten et al. (2010). The K -band surface brightnesses plotted in panel (a) were measured by Muñoz-Mateos et al. (2007) from the Two Micron All Sky Survey Extended Source Catalog (Jarrett et al. 2000). The shaded regions indicate the 1σ uncertainty in the photometry from variations in intensity within each isophote and errors in sky subtraction. The H I rotation curves were measured by Carignan & Puche (1990) and Puche et al. (1990) from Very Large Array observations of NGC 7793 and NGC 300, respectively. The shaded regions indicate the velocity uncertainties derived from the largest difference between the average radial rotation and the rotation curve measured on each side of the galaxy. Data are shown to the disk break in NGC 7793 for both the observations (~ 5.1 kpc) and simulations (~ 7.7 kpc).

40%). The artificial CMD was calculated using a 36×25 grid in $\log(\text{age}) - [Z]$ space with bin widths of 0.1 dex. We left the distance modulus and extinction free to be fitted by MATCH, which converged on a distance modulus of $m - M = 27.83$ and an extinction of $A_V = 0.05$. These are consistent with the literature values of $m - M = 27.87 \pm 0.08$ (R-S11) and $A_V = 0.06$ (Schlegel et al. 1998). We constrained the chemical enrichment history to an increasing metallicity.

The overall uncertainty in the SFH, denoted in Figure 4 by the shaded region, is a combination of both random and systematic uncertainties. The former are measured from the 1σ spread in 300 Monte Carlo realizations of the best-fit solution. The systematic uncertainties in the isochrones are calculated by varying the M_{bol} and T_{eff} values of the underlying models (for details, see Dolphin 2012).

As the simulations are only evolved for 10 Gyr, we tie their initial cumulative star formation to the equivalent value measured in NGC 7793 10 Gyr ago. The resulting SFHs of the models show a relatively smooth build up of mass. This is to be expected, as the simulations are not set in a full cosmological environment. The SFH of NGC 7793, as reconstructed from the observations, is consistent with a similar steady SFR for the life of the system.

Even though the SFHs of the two simulations are similar, they exhibit markedly different inner-disk profiles (see Figure 2). This suggests dynamical processes dominate the construction of the disk profiles, whether internally by secular processes (as in Roškar et al. 2008b) or by externally driven merger processes related to the formation of the host halo

(e.g., the two controlled simulations presented by Purcell et al. 2011). Outer-disk profiles are likely similarly affected, and in the case of the simulations presented here, they predominantly arise from radial diffusion. Figure 5 presents a direct comparison of these normalized outer-disk gradients as a function of age. There is remarkable agreement between the simulations and the NGC 7793 observations, which thus strongly attests to significant migration in NGC 7793.

4.2. Alternate Simulations

Sánchez-Blázquez et al. (2009) have also addressed radial migration in their cosmological simulations. They argue that the upturn in the age profile beyond the disk break is principally due to an extended and constant SFR in the outer disk. However, they do find evidence for some migration, and moreover have studied the outer regions of their cosmological simulations without the effects of such migration (see their Figure 17). Specifically, they found a break still formed in the radial surface brightness profiles, but without migration, the decrease in gradient of the outer-disk profile with increasing stellar age was lost.

Stellar radial migration may also be driven by other mechanisms, such as resonances between spiral structures and central bars¹¹ (Minchev & Famaey 2010), or interactions with satellites (Quillen et al. 2009; Bird et al. 2012). These processes may operate in addition to the resonant scattering from

¹¹ Although we note that resonances with the central bar are likely to have less influence on the outer disk (Debattista et al. 2006; Minchev et al. 2012).

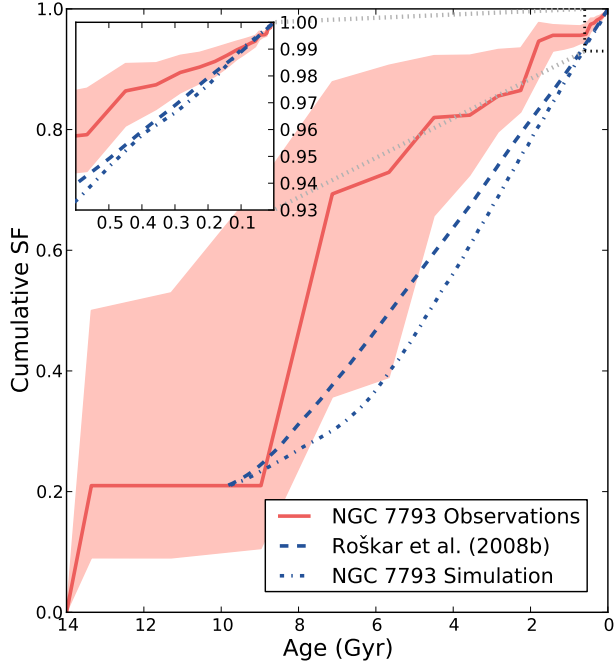


Figure 4. Comparison of the cumulative star formation history of NGC 7793 with the MW and NGC 7793 simulations as a function of age. The SFH for NGC 7793 was generated using MATCH, with the shaded region denoting the uncertainty in the measurement. As the simulations are evolved for only 10 Gyr, we fix their initial cumulative star formation to that of NGC 7793 10 Gyr ago. A zoom-in of the last 600 Myr is shown as an inset. The isolated simulations show a smooth buildup of stellar mass over the lifetime of the systems, which is consistent with the SFH reconstructed from observations of NGC 7793.

transient spiral arms, and so serve to amplify the effect. However, as NGC 7793 is not host to a significant bar, and as such features are believed to be robust (Shen & Sellwood 2004; Athanassoula et al. 2005; Debattista et al. 2006), the disk is unlikely to have been affected by a central bar. Conversely, as detailed in Section 5.3, NGC 7793 may have undergone a recent merger. Such an event could enhance spiral structure in the disk and so increase the level of stellar migration.

5. ALTERNATE EXPLANATIONS

The increase in the outer-disk scale length with stellar age, as seen in Figure 5, corresponds to an increase in the average age of the outer disk with radius. This trend, although not ubiquitous, has been confirmed using spectroscopic stellar ages in several nearby disk galaxies (Yoachim et al. 2012). To assess whether radial migration is the only viable mechanism for setting this trend, we consider alternate explanations below.

5.1. Thick Disk and Halo Contamination

The thick disk typically extends farther radially than the thin disk by a factor of 1.25, and in low-mass galaxies can account for nearly half the total mass and luminosity (Yoachim & Dalcanton 2006; Comerón et al. 2011). As the thick and thin disks can only be separated in high inclination systems, a significant portion of the older outer-disk stars may actually lie in an extended thick disk component. The smooth change in gradient of the outer radial profile with age argues against a simple two component model. However, if true, the coincident break radius of both old and young populations suggests that the mechanism propagating the break, and thus setting

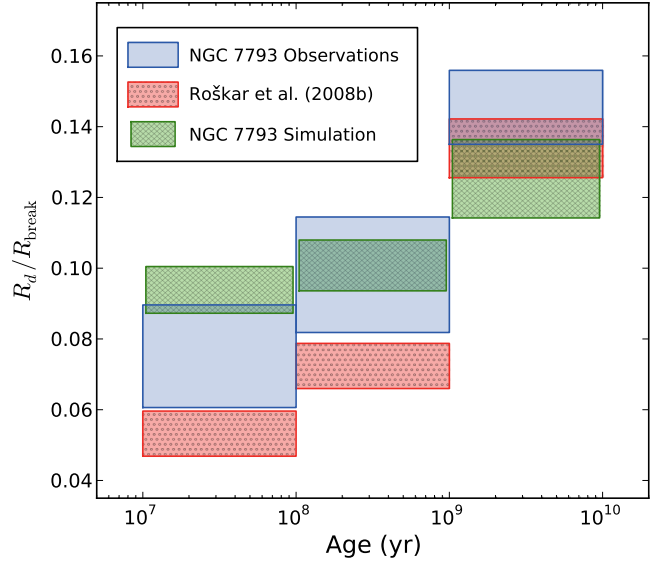


Figure 5. Comparison of the normalized exponential-disk scale lengths measured in Figure 2 for the outer disk of NGC 7793, the Roškar et al. (2008b) MW simulation, and the new NGC 7793 simulation. The width of each box represents the range of ages covered by each population, while the height encodes the 1σ uncertainty in the exponential-disk fit as calculated from Monte Carlo resamples. The width of the NGC 7793 simulation boxes are slightly reduced for clarity. Both observations and simulations argue for a smooth increase in the scale length of the outer-disk profile with stellar age.

the outer-disk gradients, applies equally to both components. Furthermore, the thick disk itself may have formed from a migrated population (Schönrich & Binney 2009; Loebman et al. 2011). Hence, contamination from a thick disk is unlikely to affect the inference of migration.

In the “Old” RGB population of NGC 7793 plotted in Figure 2, a gradual departure from the outer exponential is seen below $29 \text{ mag arcsec}^{-2}$. This may indicate a transition to either a thick disk or old stellar halo component. At $r = 11 \text{ kpc}$ ($2.2 \times R_{\text{break}}$), this extra component accounts for some $4.5 \times 10^{-3} \text{ stars arcsec}^{-2}$. This is approximately a factor of 10 greater than the number of predicted contaminants, and similar to the surface densities attributed to the stellar halos of isolated simulations of disk–satellite interactions from Purcell, Bullock & Kazantzidis (2010). However, such low numbers will have minimal impact on the exponential fits summarized in Figure 5.

5.2. In Situ Formation

Star formation in outer disks has been characterized by Bigiel et al. (2010a,b), who find evidence for spatial correlation between far-ultraviolet (FUV) emission, which traces recent star formation, and emission from atomic hydrogen gas (HI), which comprises most of the interstellar medium in the outer disk. Although Bigiel et al. (2010b) find the overall star formation efficiency to be extremely low in these regions, they observe that this efficiency scales with HI gas density. Hence, as the gas disk of NGC 7793 extends beyond the disk break, we expect some of the stars in this region to have formed in situ. This may partly account for the vertical offset seen in Figure 5 between the NGC 7793 observations and the Roškar et al. (2008b) simulation.

To explore this possibility, Figure 6 plots the surface densities of HI gas mass from the THINGS survey (Walter et al. 2008), and the SFR inferred from the GALEX Ultraviolet At-

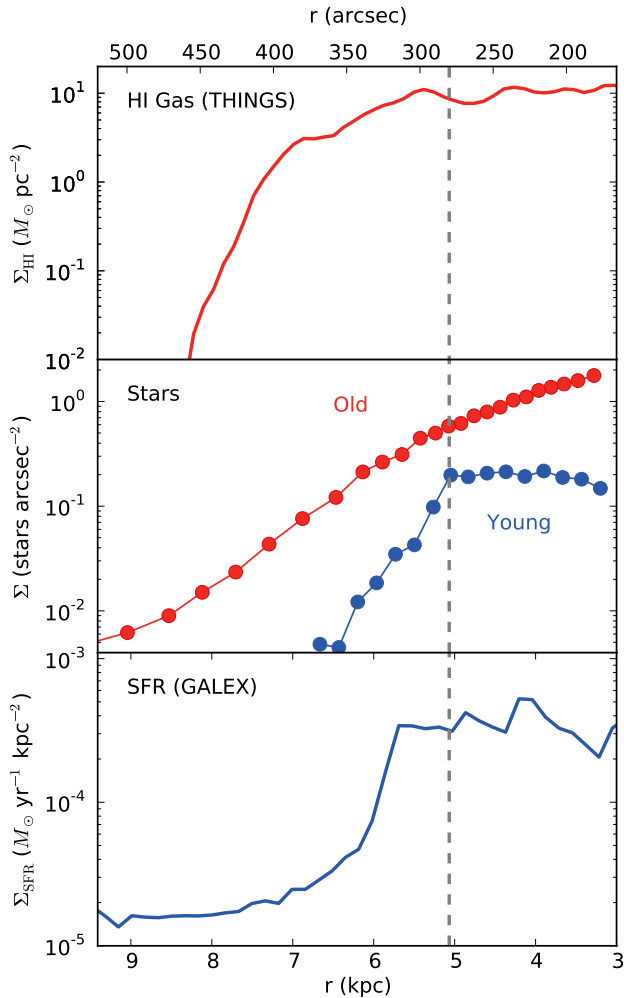


Figure 6. Top: the HI gas surface density in NGC 7793 from the THINGS survey. Middle: the star counts corresponding to the old RGB (red) and young MS and HeB (blue) profiles shown in Figure 2. Bottom: the star formation rate density from *GALEX* FUV emission. The old RGB stars are found to extend much farther than the HI disk.

las of Nearby Galaxies (Gil de Paz et al. 2007). The FUV emission does indeed extend slightly beyond the truncation. However, using *MATCH* with this inferred SFR to generate artificial CMDs underestimates the number of “Young” stars observed by almost an order of magnitude (although this calculation does carry significant uncertainties). The stars may instead have formed in previous episodes of formation not probed by the FUV flux. Indeed, the gas disk extends further still, although, as noted by Vlajić et al. (2011), the HI disk of NGC 7793 is unusually small. As shown in Figure 6, the radial extent of the gas is significantly smaller than the RGB distribution. Thus, the bulk of the old RGB stars were not likely formed in situ from the HI gas reservoir now present in the region, unless the HI disk was substantially larger in the past.

5.3. Accretion/Harassment

Many interacting systems are evident in the Local Group. Our own galaxy is tidally disrupting the Small and Large Magellanic Clouds, producing a number of phenomena such as the Magellanic Stream (Mathewson et al. 1974; Brüns et al. 2005). Such interactions strongly affect the distribution of

material in outer disks (Younger et al. 2007; Sancisi et al. 2008; Quillen et al. 2009; Bird et al. 2012; Kazantzidis et al. 2008). In the optical, NGC 7793 does not appear to be undergoing such a major merger, which would likely disrupt the outer-disk profiles. However, the HI disk of this relatively isolated galaxy is warped, and studies have revealed non-circular motions on the north side, indicative of harassment (Carignan & Puche 1990), or of an advanced stage of merging (e.g., Sancisi 1999). Such minor interactions may explain the lack of gas in the outskirts, and may lead to an extended and heated component (Purcell, Bullock & Kazantzidis 2010; Kazantzidis et al. 2009). Moreover, such interactions are also likely to induce the transient spiral features that drive stellar radial migration (Purcell, Kazantzidis & Bullock 2009; Purcell et al. 2011; Struck, Dobbs & Hwang 2011). As these transient spiral arms can last for a couple of Gyr (and potentially much longer in star-forming galaxies due to swing amplification processes involving giant molecular clouds, e.g., D’Onghia et al. 2012), the level of stellar radial migration we infer in NGC 7793 may be a direct consequence of a completed past merger.

6. SUMMARY

We have measured the radial surface brightness profiles of three distinct stellar populations across both the inner and outer disk of NGC 7793. Breaks in the radial profiles are found at the same location regardless of age. However, older stars show a steeper profile internal to the break and a shallower profile beyond the break in comparison to younger stars. The observed smooth increase in the outer-disk scale length with age suggests a formation mechanism that continually operates over a significant fraction of the lifetime of the galaxy.

We have compared the surface brightness profiles to *N*-body simulations that exhibit significant radial stellar diffusion, including a new simulation of a system comparable in mass to NGC 7793. The gradients of the outer-disk profiles in these simulations are set almost entirely by migration due to resonant scattering. The new simulation shows a slightly higher level of in situ formation beyond the disk break relative to Roškar et al. (2008b), which corresponds to a flattening of the profiles. However, the gradients overall match extremely well to the outer disk of NGC 7793.

We thus argue that the observations presented here are indicative of high levels of stellar radial migration in NGC 7793. This inference carries significant ramifications for studies of stellar populations in disk galaxies, including the MW.

Support for this work was provided by NASA through grants GO-10889 and GO-12196 from the Space Telescope Science Institute, which is operated by the Association of Universities for Research in Astronomy, Incorporated, under NASA contract NAS5-26555.

REFERENCES

- Athanassoula, E., Lambert, J. C., & Dehnen, W. 2005, *MNRAS*, 363, 496
- Bigiel, F., Leroy, A., Seibert, M., et al. 2010a, *ApJ*, 720, L31
- Bigiel, F., Leroy, A., Walter, F., et al. 2010b, *AJ*, 140, 1194
- Bird, J. C., Kazantzidis, S., & Weinberg, D. H. 2012, *MNRAS*, 420, 913
- Brüns, C., Kerp, J., Staveley-Smith, L., et al. 2005, *A&A*, 432, 45
- Carignan, C., & Puche, D. 1990, *AJ*, 100, 394
- Comerón, S., Elmegreen, B. G., Knapen, J. H., et al. 2011, *ApJ*, 741, 28
- de Jong, R. S., Seth, A. C., Rada-Burn-Smith, D. J., et al. 2007, *ApJ*, 667, L49
- Debatista, V. P., Mayer, L., Carollo, C. M., et al. 2006, *ApJ*, 645, 209
- Dehnen, W., & Binney, J. J. 1998, *MNRAS*, 298, 387
- Dolphin, A. E. 2000, *PASP*, 112, 1383

- Dolphin, A. E. 2002, *MNRAS*, 332, 91
- Dolphin, A. E. 2012, *ApJ*, 751, 60
- D’Onghia, E., Vogelsberger, M., & Hernquist, L. 2012, arXiv:1204.0513
- Edvardsson, B., Andersen, J., Gustafsson, B., et al. 1993, *A&A*, 275, 101
- Ellis, S. C. & Bland-Hawthorn, J. 2007, *MNRAS*, 377, 815
- Elmegreen, B. G., & Hunter, D. A. 2006, *ApJ*, 636, 712
- Gil de Paz, A., Boissier, S., Madore, B. F., et al. 2007, *ApJS*, 173, 185
- Girardi, L., Bertelli, G., Bressan, A., et al. 2002, *A&A*, 391, 195
- Girardi, L., Williams, B. F., Gilbert, K. M., et al. 2010, *ApJ*, 724, 1030
- Gogarten, S. M., Dalcanton, J. J., Williams, B. F., et al. 2010, *ApJ*, 712, 858
- Jarrett, T. H., Chester, T., Cutri, R., et al. 2000, *AJ*, 119, 2498
- Kazantzidis, S., Bullock, J. S., Zentner, A. R., Kravtsov, A. V., & Moustakas, L. A. 2008, *ApJ*, 688, 254
- Kazantzidis, S., Zentner, A. R., Kravtsov, A. V., Bullock, J. S., & Debattista, V. P. 2009, *ApJ*, 700, 1896
- Kennicutt, R. C., Jr. 1989, *ApJ*, 344, 685
- Loebman, S. R., Roškar, R., Debattista, V. P., et al. 2011, *ApJ*, 737, 8
- Marigo, P., Girardi, L., Bressan, A., et al. 2008, *A&A*, 482, 883
- Mathewson, D. S., Cleary, M. N., & Murray, J. D. 1974, *ApJ*, 190, 291
- Minchev, I., & Famaey, B., 2010, *ApJ*, 722, 112
- Minchev, I., Famaey, B., Quillen, A. C., et al. 2012, arXiv:1203.2621
- Muñoz-Mateos, J. C., Gil de Paz, A., Boissier, S., et al. 2007, *ApJ*, 658, 1006
- Muñoz-Mateos, J. C., Gil de Paz, A., Zamorano, J., et al. 2009, *ApJ*, 703, 1569
- Pohlen, M., & Trujillo, I. 2006, *A&A*, 454, 759
- Puche, D., Carignan, C., & Bosma, A. 1990, *AJ*, 100, 1468
- Purcell, C. W., Bullock, J. S., & Kazantzidis, S. 2010, *MNRAS*, 404, 1711
- Purcell, C. W., Bullock, J. S., Tollerud, E. J., Rocha, M., & Chakrabarti, S. 2011, *Nature*, 477, 301
- Purcell, C. W., Kazantzidis, S., & Bullock, J. S. 2009, *ApJL*, 694, L98
- Quillen, A. C., Minchev, I., Bland-Hawthorn, J., & Haywood, M. 2009, *MNRAS*, 397, 1599
- Radburn-Smith, D. J., de Jong, R. S., Seth, A. C., et al. 2011, *ApJS*, 195, 18
- Roškar, R., Debattista, V. P., Quinn, T. R., Stinson, G. S., & Wadsley, J. 2008a, *ApJ*, 684, L79
- Roškar, R., Debattista, V. P., Stinson, G. S., et al. 2008b, *ApJ*, 675, L65
- Salpeter, E. E. 1955, *ApJ*, 121, 161
- Sánchez-Blázquez, P., Courty, S., Gibson, B. K., & Brook, C. B. 2009, *MNRAS*, 398, 591
- Sancisi, R. 1999, *Ap&SS*, 269, 59
- Sancisi, R., Fraternali, F., Oosterloo, T., & van der Hulst, T. 2008, *A&AR*, 15, 189
- Schaye, J. 2004, *ApJ*, 609, 667
- Schlegel, D. J., Finkbeiner, D. P., & Davis, M. 1998, *ApJ*, 500, 525
- Schönrich, R., & Binney, J. 2009, *MNRAS*, 396, 203
- Sellwood, J. A., & Binney, J. J. 2002, *MNRAS*, 336, 785
- Sellwood, J. A., & Carlberg, R. G. 1984, *ApJ*, 282, 61
- Shen, J., & Sellwood, J. A. 2004, *ApJ*, 604, 614
- Struck, C., Dobbs, C. L., & Hwang, J.-S. 2011, *MNRAS*, 414, 2498
- Trujillo, I., & Pohlen, M. 2005, *ApJ*, 630, L17
- van der Kruit, P. C., & Searle, L. 1981, *A&A*, 95, 105
- Vlajić, M., Bland-Hawthorn, J., & Freeman, K. C. 2011, *ApJ*, 732, 7
- Walter, F., Brinks, E., de Blok, W. J. G., et al. 2008, *AJ*, 136, 2563
- Wielen, R. 1977, *A&A*, 60, 263
- Williams, B. F., Dalcanton, J. J., Dolphin, A. E., Holtzman, J., & Sarajedini, A. 2009, *ApJL*, 695, L15
- Yoachim, P., & Dalcanton, J. J. 2006, *AJ*, 131, 226
- Yoachim, P., Roškar, R., & Debattista, V. P. 2012, *ApJ*, 752, 97
- Younger, J. D., Cox, T. J., Seth, A. C., & Hernquist, L. 2007, *ApJ*, 670, 269